Incorporating source directivity in wave-based virtual acoustics

Incorporating Source Directivity in Wave-based Virtual Acoustics: Time-domain Models and Fitting to Measured Data

Stefan Bilbao,[1] Jens Ahrens,[2] and Brian Hamilton[1]
[1] *Acoustics and Audio Group/Reid School of Music, University of Edinburgh, Edinburgh, United Kingdom*
[2] *Audio Technology Group, Division of Applied Acoustics, Chalmers University of Technology, 412 96 Gothenburg, Sweden*

(Dated: 1 October 2019)

The modeling of source directivity is a problem of longstanding interest in virtual acoustics and auralisation. This remains the case for newer time domain volumetric wave-based approaches to simulation such as the finite difference time domain (FDTD) method. In this article, a spatio-temporal model of acoustic wave propagation, including a source term is presented. The source is modeled as a spatial Dirac delta function under the action of a series of differential operators associated with the spherical harmonic functions. Each term in the series gives rise to the directivity pattern of a given spherical harmonic, and is separately driven through a time domain filtering operation of an underlying source signal. Such a model is suitable for calibration against measured frequency-dependent directivity patterns and a procedure for arriving at time domain filters for each spherical harmonic channel is illustrated. It also yields a convenient framework for discretisation, and a simple strategy is presented, yielding a locally-defined operation over the spatial grid. Numerical results, illustrating various features of source directivity, including the comparison of measured and synthetic directivity patterns are presented. [a]

 [http://dx.doi.org(DOI number)]

[XYZ] Pages: 1–13

The following article has been accepted for publication in the Journal of the Acoustical Society of America. After it is published, it will be found at `http://asa.scitation.org/journal/jas`

I. INTRODUCTION

The modeling and computer simulation of source directivity is a subject of longstanding interest particularly in the domain of concert hall acoustics, and also in virtual acoustics applications. Currently, most geometrical room acoustics simulation packages include a means of incorporating at least simple source directivities[1], based, for example, on the Common Loudspeaker Format[2]; see also the discussion of source directivity in geometrical acoustics in the review paper by Savioja and Svensson[3]. Spherical harmonic representations of sound source directivity[4] have become increasingly common, particularly since the work of Zotter[5] and are sometimes referred to as *O-format* in the Ambisonics community[6,7]. This has allowed for the incorporation of source directivity into virtual acoustics[8,9], and publicly available databases have been created[10]. Sound source directivity has also been employed in geometric room simulations based on the spherical harmonic representation[11,12].

Time-domain wave-based volumetric approaches to acoustic simulation have increased in sophistication and their range of applications since the first work in the mid 1990s[13–16]. The finite difference time domain method (FDTD) is the best-known example, but other equivalent or related methods, including finite volume methods[17,18], pseudospectral methods[19,20] and the digital waveguide mesh[21] have also been employed. It is such volumetric methods which will be discussed in this article. Non-volumetric frequency domain methods (such as the boundary element method[22]) are also classified as wave-based, but will not be considered here.

Source modeling in volumetric wave-based methods has mostly focussed on the problem of simple omnidirectional[23–25] and dipole sources[26–28], particularly with regard to the distinction between hard, soft and transparent sources[29]. There have been approaches to the modeling of complex directivity patterns using collections of monopole sources[30] or through the matching of initial values over the simulation domain[31].

In recent work, source models have been framed through the use of the wave equation accompanied by an additional term containing the three-dimensional (3D) Dirac delta function under the action of a series of Carte-

[a] Portions of this work appear in *Local Directional Source Modeling in Wave-based Acoustic Simulation*, S. Bilbao, J. Ahrens and B. Hamilton, Proceedings of the International Congress on Acoustics, Aachen, Germany, 2019.

sian spatial differential operators. In particular, the multipole representation has been employed, both in acoustics applications[32] and in more general settings[33]. A more natural approach is to associate such differential operators in Cartesian coordinates with spherical harmonic directivity patterns. This is in contrast to the case of the multipole expansion, where the directivity corresponding to each term is frequency dependent.

In a representation fleetingly used in sound-field microphone capture, due to Dickins[34,35], but which can be traced back to much earlier work in electromagnetics[36], the spherical harmonic expansion of the acoustic field at a given location may be represented through a series of Cartesian spatial derivatives of the acoustic field at a single location. Such a model has been used as the basis for ambisonic output in virtual acoustics applications, using FDTD[37] as well as boundary element techniques[38]. The dual case of the point-like source with arbitrary directivity is presented here; due to the spherical harmonic representation of the source term, fitting to measured data is greatly simplified compared with the multipole representation, and due to the representation of spherical harmonic differential operators in Cartesian coordinates, the translation to a discrete setting such as FDTD is direct. In essence, the model presented here allows for a useful context-free division of the source model into spatial and temporal parts which can ultimately be approached separately in a numerical setting.

A generalised partial differential equation model of a point source with arbitrary directivity is presented in Section II. It is written entirely in the spatio-temporal domain, and the source is modeled through a Dirac distribution under the action of a set of differential operators, each of which is associated with a particular spherical harmonic directivity pattern. The special case of the displaced monopole source is described in Section III. Such a framework allows for direct fitting of a spatio-temporal model to measured source directivity, as shown in Section IV. Volumetric time domain methods are introduced in Section V, accompanied by simple strategies for the discretisation of the Dirac distribution under spatial differentiation. Numerical results, illustrating individual spherical harmonic directivities, the displaced monopole, and for sources fit to measured directivity data appear in Section VI. Concluding remarks appear in Section VII.

II. SOURCE MODELS

This article is concerned with source modeling for the 3D wave equation, defined as[39]

$$\frac{1}{c^2}\partial_t^2 p - \Delta p = 0\,. \tag{1}$$

Here, $p\,(\mathbf{r},t)$ is the acoustic pressure, in Pa, as a function of time $t \in \mathbb{R}$, in s and spatial coordinate $\mathbf{r} = [x,\, y,\, z]$, in m. c is the wave speed, in m$\cdot$ s^{-1}. Here and henceforth in this article, we will use $\mathbf{r} = r\boldsymbol{\gamma}$, where r is a scalar distance, and where $\boldsymbol{\gamma}$ is a unit-length vector representing direction. ∂_t represents partial differentiation with respect to time t, and Δ is the 3D Laplacian, defined as $\Delta = \nabla\cdot\nabla$ in terms of the gradient ∇, where

$$\nabla = [\partial_x,\, \partial_y,\, \partial_z]\,. \tag{2}$$

The operator ∂_ν represents partial spatial differentiation with respect to coordinate ν, $\nu = x, y, z$.

As the interest is in localised source modeling, wall conditions are not considered, and thus $\mathbf{r} \in \mathbb{R}^3$; in the context of volumetric wave-based numerical methods, such wall conditions may be considered locally, and separately from the source itself, provided the source is sufficiently distant from any domain boundary. As the interest here is in forced solutions of the wave equation (1), it is assumed defined here over all t, so that initial conditions need not be considered.

A. The Monopole and Dipole

A standard model of a source is through the introduction of additional driving terms on the right-hand side of (1). A basic example is the monopole[40], defined as

$$\frac{1}{c^2}\partial_t^2 p - \Delta p = f(t)\delta^{(3)}\left(\mathbf{r}\right)\,. \tag{3}$$

Here, $f\,(t)$ is a forcing function, equal to $\rho\dot{Q}$, where ρ is air density, and $Q\,(t)$ is a point source volume velocity (and $\dot{Q}$ its ordinary time derivative). $\delta^{(3)}\left(\mathbf{r}\right)$ is a 3D Dirac delta function selecting the source location $\mathbf{r} = \mathbf{0}$. In this article, with little loss in generality, the source is assumed to lie at coordinates $\mathbf{r} = \mathbf{0}$. Such a model injects energy into the acoustic field, and does not otherwise interact with it—this is in contrast to so-called hard-source models, where such an interaction is possible[29].

The solution to (3) is

$$p(\mathbf{r},t) = \frac{f(t - r/c)}{4\pi r}\,. \tag{4}$$

Under Fourier transformation (see Appendix A), the solution $\hat{p}\,(\mathbf{r},\omega)$ may be written, in terms of angular frequency ω, as

$$\hat{p}\,(\mathbf{r},\omega) = \hat{f}\frac{e^{i\omega r/c}}{4\pi r} = \hat{f}\frac{i\omega}{4\pi c}h_0^{(1)}\left(\omega r/c\right)\,. \tag{5}$$

$\hat{f}\,(\omega)$ is the Fourier transform of $f(t)$, and $h_0^{(1)}$ is the zeroth order spherical Hankel function of the first kind.

A point model of a dipole[40] may also be written using a Dirac distribution, now under directional spatial differentiation:

$$\frac{1}{c^2}\partial_t^2 p - \Delta p = f(t)\left(\mathbf{n}\cdot\nabla\right)\delta^{(3)}\left(\mathbf{r}\right)\,. \tag{6}$$

Here, $f(t)$ is a point driving force (in N), acting in direction $-\mathbf{n}$, for a unit-length 3-vector $\mathbf{n}$. The solution is

$$p\,(\mathbf{r},t) = -\frac{(\mathbf{n}\cdot\boldsymbol{\gamma})}{4\pi r^2}\left((r/c)\dot{f}\,(t - r/c) + f\,(t - r/c)\right)\,, \tag{7}$$

where $\dot{f}$ is the ordinary time derivative of f. Under Fourier transformation, the solution $\hat{p}$ is

$$\hat{p}\left(\mathbf{r},\omega\right)=-i\left(\mathbf{n}\cdot\boldsymbol{\gamma}\right)\hat{f}\frac{\omega^2}{4\pi c^2}h_1^{(1)}\left(\omega r/c\right)\,. \tag{8}$$

Using source terms involving repeated differentiation of the Dirac delta function, one may construct a multipole expansion for the source[32,33]. For a multipole of order higher than one, however, directivity is in general dependent on frequency—the longitudinal quadrupole being the simplest such example. Another approach is to make use of differential operators derived from spherical harmonics, which will allow a decomposition of the field better suited to calibration against measured directivity.

B. Spherical Harmonics and Associated Differential Operators

The spherical harmonic functions $Y_{l,m}\left(\alpha,\beta\right)$, defined for integer $l\geq 0$ and m with $-l\leq m\leq l$, are normally written as a function of two angles: an azimuthal angle α, with $0\leq\alpha<2\pi$ and an inclination angle β, with $0\leq\beta\leq\pi$[39]. In this work, the functions $Y_{l,m}$ are assumed real, and normalised over the unit sphere S^2:

$$\iint_{S^2}Y_{l,m}\left(\alpha,\beta\right)Y_{l',m'}\left(\alpha,\beta\right)d\Omega=\begin{cases}1, & l=l',m=m'\\ 0, & \text{otherwise}\end{cases}\,, \tag{9}$$

where the surface differential element $d\Omega=\sin\left(\beta\right)d\beta d\alpha$.

Alternatively, $Y_{l,m}$ may be written in terms of a unit-length 3-vector $\boldsymbol{\gamma}$

$$\boldsymbol{\gamma}=\left[\gamma_x,\,\gamma_y,\,\gamma_z\right]=\left[\sin\left(\beta\right)\cos\left(\alpha\right),\,\sin\left(\beta\right)\sin\left(\alpha\right),\,\cos\left(\beta\right)\right]. \tag{10}$$

The $Y_{l,m}$ are then homogeneous polynomials of degree l in γ_x, γ_y and γ_z. Expressions for $Y_{l,m}$ up to $l=2$ are shown in Table I.

An associated differential operator $D_{l,m}$ may be defined[36,37] as

$$D_{l,m}=Y_{l,m}\left(\nabla\right)\,, \tag{11}$$

where $Y_{l,m}$ takes the gradient operator ∇, from (2) as its argument. For example:

$$D_{0,0}=\tfrac{1}{\sqrt{4\pi}}\quad D_{1,-1}=\sqrt{\tfrac{3}{4\pi}}\partial_y\quad D_{2,2}=\sqrt{\tfrac{15}{16\pi}}\left(\partial_x^2-\partial_y^2\right)\,. \tag{12}$$

In general, the operator $D_{l,m}$ may be written in the form

$$D_{l,m}=\sum_{\boldsymbol{\eta}\in\mathbb{B}^l}\sigma_{l,m}^{(\boldsymbol{\eta})}\prod_{\nu=x,y,z}\partial_\nu^{\eta_\nu}\,, \tag{13}$$

for some coefficients $\sigma_{l,m}^{(\boldsymbol{\eta})}$ indexed by $\boldsymbol{\eta}=[\eta_x,\eta_y,\eta_z]\in\mathbb{B}^l$, where $\mathbb{B}^l$ indicates the set of non-negative integer-valued three vectors whose components sum to l.

C. A Generalized Source Model

Consider the following model, generalising (3) and (6) above:

$$\frac{1}{c^2}\partial_t^2 p-\Delta p=\sum_{l=0}^{\infty}\sum_{m=-l}^{l}c^l f_{l,m}(t)D_{l,m}\delta^{(3)}\left(\mathbf{r}\right)\,. \tag{14}$$

Each term in the double sum in (14) above activates a directivity pattern associated with one of the spherical harmonics, as will be seen shortly, through the application of the differential operator $D_{l,m}$, as defined in (11) to the Dirac delta function. The relative strength of the (l,m)th pattern in the resulting complete directivity pattern (which is, in general, frequency dependent) is determined by the associated driving function $f_{l,m}(t)$. A general modeling approach is to relate such driving functions back to a scalar driving function $f\left(t\right)$ through convolution with the functions $a_{l,m}\left(t\right)$, as

$$f_{l,m}\left(t\right)=a_{l,m}(t)*f(t)\,. \tag{15}$$

It is thus the functions $a_{l,m}$ which determine the frequency-dependent source directivity.

The general solution to (14) may be obtained, using superposition, from the solution to the monopole from (4):

$$p\left(\mathbf{r},t\right)=\sum_{l=0}^{\infty}\sum_{m=-l}^{l}c^l D_{l,m}\left(\frac{f_{l,m}(t-r/c)}{4\pi r}\right)\,. \tag{16}$$

The Fourier transformed solution may be determined using the solution for the monopole, from (5):

$$\hat{p}\left(\mathbf{r},\omega\right)=\frac{i\omega}{4\pi c}\sum_{l=0}^{\infty}\sum_{m=-l}^{l}c^l\hat{f}_{l,m}\left(\omega\right)D_{l,m}h_0^{(1)}\left(\omega r/c\right)\,. \tag{17}$$

But, using the identity (B1) from Appendix B leads to

$$\hat{p}=\frac{i\omega}{4\pi c}\sum_{l=0}^{\infty}\sum_{m=-l}^{l}\left(-\omega\right)^l\hat{f}_{l,m}Y_{l,m}\left(\boldsymbol{\gamma}\right)h_l^{(1)}\left(\omega r/c\right)\,. \tag{18}$$

Considering now a scalar source $f(t)$, driving system (14) through the application of filters $a_{l,m}(t)$ through (15). Under Fourier transformation, (15) becomes $\hat{f}_{l,m}\left(\omega\right)=\hat{a}_{l,m}\left(\omega\right)\hat{f}\left(\omega\right)$, where $\hat{a}_{l,m}\left(\omega\right)$ are the Fourier transforms of the filter responses $a_{l,m}(t)$. Inserting this expression in (18) gives

$$\hat{p}=\frac{i\omega}{4\pi c}\hat{f}\sum_{l=0}^{\infty}\sum_{m=-l}^{l}\left(-\omega\right)^l\hat{a}_{l,m}Y_{l,m}\left(\boldsymbol{\gamma}\right)h_l^{(1)}\left(\omega r/c\right)\,. \tag{19}$$

Such an expression recovers the general form of the solution to the wave equation for an exterior problem[41]. The model given in (14), however, is directly suitable for discretisation in the spatio-temporal domain (see Section V), and will serve as the basis for the simulation results presented in Section VI.

TABLE I. $Y_{l,m}(\boldsymbol{\gamma})$ for $l = 0, 1, 2$ in Cartesian form.

$l \backslash m$	-2	-1	0	1	2
0	·	·	$\sqrt{1/4\pi}$	·	·
1	·	$\sqrt{3/4\pi}\gamma_y$	$\sqrt{3/4\pi}\gamma_z$	$\sqrt{3/4\pi}\gamma_x$	·
2	$\sqrt{15/4\pi}\gamma_x\gamma_y$	$\sqrt{15/4\pi}\gamma_y\gamma_z$	$\sqrt{5/16\pi}\left(2\gamma_z^2-\gamma_x^2-\gamma_y^2\right)$	$\sqrt{15/4\pi}\gamma_x\gamma_z$	$\sqrt{15/16\pi}\left(\gamma_x^2-\gamma_y^2\right)$

III. EXAMPLE: DISPLACED MONOPOLE

A useful test case, showing the ability of the localised time-domain source model (14) to reproduce near-field effects is that of the displaced monopole source. The defining equation is

$$\frac{1}{c^2}\partial_t^2 p - \Delta p = f(t)\delta^{(3)}(\mathbf{r}-\mathbf{r}_0)\,. \tag{20}$$

Here, as in the case of the monopole at $\mathbf{r} = \mathbf{0}$ from (3), $f(t)$ is the source strength, but the monopole is now located at $\mathbf{r} = \mathbf{r}_0$, where $\mathbf{r}_0 = r_0\boldsymbol{\gamma}_0$, for a source distance r_0 and unit-length direction vector $\boldsymbol{\gamma}_0$. The solution is

$$p(\mathbf{r},t) = \frac{f(t-|\mathbf{r}-\mathbf{r}_0|/c)}{4\pi|\mathbf{r}-\mathbf{r}_0|}\,. \tag{21}$$

Under Fourier transformation, the solution $\hat{p}(\mathbf{r},\omega)$ may be written as

$$\hat{p}(\mathbf{r},\omega) = \hat{f}(\omega)\frac{e^{i\omega|\mathbf{r}-\mathbf{r}_0|/c}}{4\pi|\mathbf{r}-\mathbf{r}_0|}\,, \tag{22}$$

or, expanding onto spherical harmonics[42], as

$$\hat{p} = \frac{i\omega\hat{f}}{c}\sum_{l=0}^{\infty}\sum_{m=-l}^{l} j_l(\omega t_0)\,Y_{l,m}(\boldsymbol{\gamma}_0)\,h_l^{(1)}(\omega r/c)\,Y_{l,m}(\boldsymbol{\gamma})\,, \tag{23}$$

where here, $t_0 = r_0/c$ is the time of travel between the source location and the coordinate centre, and j_l is the lth order spherical Bessel function.

Through comparison with the Fourier-transformed solution (18) to the model system (14), one may arrive at the following identification for the filters $\hat{a}_{l,m}$:

$$\hat{a}_{l,m} = 4\pi(-1)^l Y_{l,m}(\boldsymbol{\gamma}_0)\frac{j_l(\omega t_0)}{\omega^l}\,. \tag{24}$$

A. Time-domain Filter Expressions

It is possible to arrive at simple closed-form expressions for the filter responses $a_{l,m}(t)$ in the following way. Consider the frequency domain expression appearing in (24):

$$\hat{q}_l(\omega) = \frac{j_l(\omega t_0)}{\omega^l}\,. \tag{25}$$

Using the identity:

$$j_l(\xi) = (-1)^l\xi^l\left(\frac{1}{\xi}\frac{d}{d\xi}\right)^l j_0(\xi)\,, \tag{26}$$

we have

$$\hat{q}_l(\omega) = \left(-\frac{1}{\omega t_0}\frac{d}{d\omega}\right)^l j_0(\omega t_0)\,. \tag{27}$$

This can be framed, recursively, as

$$\hat{q}_0(\omega) = j_0(\omega t_0) \qquad \hat{q}_{l+1}(\omega) = -\frac{1}{\omega t_0}\frac{d}{d\omega}\hat{q}_l(\omega)\,. \tag{28}$$

The recursion in (28) may be written, in the time domain, as

$$q_0(t) = \frac{1}{2t_0}\sqcap(t/t_0) \qquad q_{l+1}(t) = -\frac{1}{t_0}\int_{-\infty}^{t} t' q_l(t')\,dt'\,, \tag{29}$$

where the box function $\sqcap(\xi)$ is defined as

$$\sqcap(\xi) = \begin{cases} 1, & |\xi| \le 1 \\ 0, & |\xi| > 1 \end{cases}\,. \tag{30}$$

The closed form expressions

$$q_l(t) = \frac{t_0^{l-1}}{2\cdot(2l)!!}\left(1-\frac{t^2}{t_0^2}\right)^l\sqcap(t/t_0) \tag{31}$$

result. See Figure 1.

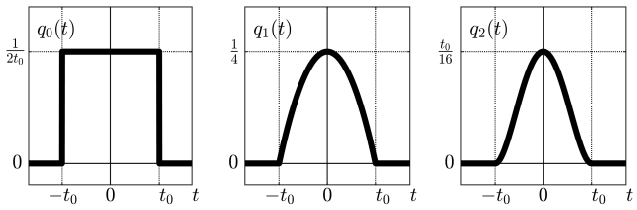

FIG. 1. The functions $q_l(t)$, for $l = 0, 1, 2$.

Finally, the time domain forms of the resulting filter responses may be written as

$$a_{l,m}(t) = 4\pi(-1)^l Y_{l,m}(\boldsymbol{\gamma}_0)\,q_l(t)\,. \tag{32}$$

Note that these are all time-limited to the interval $-t_0 \le t \le t_0$, and are polynomial over this interval. This suggests simple FIR forms in a discrete time implementation, though some latency is unavoidable due to the non-causal filter responses of $a_{l,m}(t)$. See Section VI B for

time domain simulation results illustrating the response of the displaced monopole. Related time domain forms have appeared, through inverse Fourier transformation of the spherical Bessel function, in the context of sound-field microphones[43], and can be related back to Legendre polynomials through Rodrigues' formula[44].

IV. FITTING TO MEASURED DATA

The term *directivity* takes on a variety of related meanings in the literature. Early works refer to the direction and frequency-dependent radiated magnitude evaluated at a given finite distance, as in for example, Meyer[45]; in the Common Loudspeaker Format[2], directivity refers to the radiated magnitude smoothed over fractional octave bands; Blackstock[46] refers to the radiated magnitude relative to the direction of maximum radiation; and Williams[47] (p. 204) uses the term directivity pattern to refer to the spatio-temporal transfer function (STTF) of the sound source evaluated at infinity.

All such definitions discard some information on source radiation. We therefore define directivity as the STTF of a sound source under free-field conditions. This is the most general definition, from which the other definitions above can be derived. The STTF may be evaluated at arbitrary spatial locations. Here, we will assume that the directivity is evaluated on a spherical surface centered around the source. Formally, for the source model described in Section II, we may define the directivity $W_{\text{model}} = W_{\text{model}}(\mathbf{r}, \omega)$ as

$$W_{\text{model}} \propto \frac{\hat{p}}{\hat{f}} = \frac{i\omega}{4\pi c} \sum_{l=0}^{\infty} \sum_{m=-l}^{l} (-\omega)^l \, \hat{a}_{l,m} Y_{l,m}(\boldsymbol{\gamma}) \, h_l^{(1)}(\omega r/c) \, . \tag{33}$$

Here, the proportionality constant $\propto$ indicates that, in general when working with measured directivities, we will not have access to the precise physical units. Directivities are usually measured in terms electrical voltages, for example of microphone signals, so that a calibration to sound pressure is required. In what follows, then, we will simply assume that $W_{\text{model}} = \hat{p}/\hat{f}$, with calibration to be performed as necessary.

A measured directivity $W(R, \boldsymbol{\gamma}, \omega)$ that is known on a continuous spherical surface of radius R that includes the source in its complete physical extent can be represented via its spherical harmonic coefficients $\breve{W}_{l,m}(R, \omega)$ as[47]

$$W(R, \boldsymbol{\gamma}, \omega) = \sum_{l=0}^{\infty} \sum_{m=-l}^{l} \underbrace{\breve{W}_{l,m}(\omega) h_l^{(1)}(\omega R/c)}_{\mathring{W}_{l,m}(R,\omega)} Y_{l,m}(\boldsymbol{\gamma}) \, . \tag{34}$$

The spatial-temporal transfer function $W(\mathbf{r}, \omega)$ of the source to any arbitrary location $\mathbf{r}$ is then

$$W(\mathbf{r}, \omega) = \sum_{l=0}^{\infty} \sum_{m=-l}^{l} \frac{\mathring{W}_{l,m}(R, \omega)}{h_l^{(1)}\left(\frac{\omega R}{c}\right)} \, h_l^{(1)}(\omega r/c) \; Y_{l,m}(\boldsymbol{\gamma}) \, . \tag{35}$$

Comparing (35) to (33) shows that the functions $\hat{a}_{l,m}(\omega)$ can be computed from the coefficients $\mathring{W}_{l,m}(R, \omega)$ of the source directivity as

$$\hat{a}_{l,m}(\omega) = \frac{4\pi c \, (-1)^l \, i^l}{(i\omega)^{l+1} h_l^{(1)}\left(\frac{\omega R}{c}\right)} \, \mathring{W}_{l,m}(R, \omega) \, . \tag{36}$$

The fraction on the right-hand side of (36) deserves further attention. It constitutes a filter that is applied to the coefficients $\mathring{W}_{l,m}(R, \omega)$. The Hankel function $h_l^{(1)}(\zeta)$ can be represented as[39]

$$h_l^{(1)}(\zeta) = i^{-l-1} \frac{e^{i\zeta}}{\zeta} \sum_{n=0}^{l} \frac{(l+n)!}{n!(l-n)!} \left(-\frac{1}{2i\zeta}\right)^n \, , \tag{37}$$

which makes it clear that it contains a delay (the complex exponential). Dividing by the Hankel function in (36) is equivalent to an anticipation by the propagation time of the sound from the center of the measurement sphere to the sphere. It is therefore important that the coefficients $\mathring{W}_{l,m}(R, \omega)$ contain this delay to maintain causality. We refer the reader to[48,49] for recursive implementations of expressions that are similar to (36).

The coefficients $\mathring{W}_{l,m}(R, \omega)$ in (36) can be obtained from measurement data in two different ways: 1) discretization of the transformation integral, or 2) numerical fitting, as explained below. Practical constraints require approximating (35) by limiting the order l to L. One then speaks of an L-th order directivity; approximations up to order $L = 10$ are common in practice.

The transformation integral, i.e., the operation that is inverse to (34), reads[47] (p. 207)

$$\breve{W}_{l,m}(\omega) = \frac{1}{h_l^{(1)}\left(\frac{\omega R}{c}\right)} \iint_{S^2} W(R, \boldsymbol{\gamma}, \omega) \, Y_{l,m}(\boldsymbol{\gamma}) d\Omega \, , \tag{38}$$

Eq. (38) requires that the directivity is known along a continuous surface, which is not possible in practice. The integral has to be discretized, whereby quadrature weights that depend on the sampling grid have to be employed to maintain orthogonality of the spherical harmonics basis functions[50].

The alternative to (38) is performing a numerical fit. To achieve this, (34) is interpreted as a linear system of equations[51] relating a finite set of spherical harmonic coefficients to a finite set of sampled measurements of $W(R, \boldsymbol{\gamma}, \omega)$ over the sphere. Noting that the coefficients $\mathring{W}_{l,m}(R, \omega)$ are the same in all equations for a given frequency establishes a non-square system of linear equations with $(L+1)^2$ unknown coefficients $\mathring{W}_{l,m}(R, \omega)$. This

equation system is solved for each frequency separately, for example, by means of the Moore-Penrose pseudo inverse[52], which yields a least-squares fit. The memory requirements and computational cost for this process are moderate, but independent of any subsequent numerical discretisation approach for the model itself.

V. VOLUMETRIC WAVE-BASED SIMULATION

The source model given in (14), expressed entirely in the spatio-temporal domain is intended for general use within a volumetric time domain simulation method. For the sake of illustration, only the most basic finite difference time domain method will be employed in this article.

A. Basic Scheme

Let $p_{\mathbf{q}}^n$ represent an approximation to $p(\mathbf{r}, t)$, at time $t = nT$ and spatial location $\mathbf{r} = \mathbf{q}X$, for integer n and integer 3-tuples $\mathbf{q} \in \mathbb{Z}^3$. Here, X, in m, is the grid spacing, and T is the time step, in s (and the sample rate is $1/T$).

A basic explicit scheme for the 3D wave equation (1), sometimes referred to as the seven-point scheme, may be written as

$$p_{\mathbf{q}}^{n+1} = 2p_{\mathbf{q}}^n - p_{\mathbf{q}}^{n-1} + \lambda^2 \sum_{\mathbf{e}\in\mathbb{Q}} \left(p_{\mathbf{q}+\mathbf{e}}^n - p_{\mathbf{q}}^n\right) , \tag{39}$$

where

$$\mathbb{Q} = \{\mathbf{e} \in \mathbb{Z}^3 | \|\mathbf{e}\|_1 = 1\} , \tag{40}$$

and where

$$\lambda = cT/X \tag{41}$$

is the Courant number for the scheme. For this simple scheme, the Courant number must be bounded from above as $\lambda \leq 1/\sqrt{3}$ (the Courant-Friedrichs-Lewy condition[53]). In this work, we will take $\lambda = 1/\sqrt{3}$.

The scheme in (39) is the simplest available—at a given grid point, the update is performed using values at the six neighbours. It also suffers from numerical dispersion[54]; explicit methods with greatly reduced dispersion have been proposed[55], including in the present context of source modeling[32].

B. Source Terms

Consider the discrete representation of the 3D Dirac delta function $\delta^{(3)}(\mathbf{r})$ over a grid of spacing X. The obvious approximation is a grid function $s_{\mathbf{q}}$, defined by

$$s_{\mathbf{q}} = \begin{cases} 1/X^3, & \mathbf{q} = \mathbf{0} \\ 0, & \text{otherwise} \end{cases} . \tag{42}$$

In order to approximate the series of terms in (14), consider any individual operator $D_{l,m}$, in the general form in (13), consisting of a weighted sum of products of powers of spatial differential operators ∂_ν, $\nu = x, y, z$. These may be approximated, in an FDTD setting, using combinations of spatial shift operators defined over the grid. For a general grid function $g_{\mathbf{q}}$, forwards and backwards shifts in the ν direction are defined as

$$e_\nu^+ g_{\mathbf{q}} = g_{\mathbf{q}+\mathbf{e}_\nu} \qquad e_\nu^- g_{\mathbf{q}} = g_{\mathbf{q}-\mathbf{e}_\nu} , \tag{43}$$

where $\mathbf{e}_\nu$ is a unit vector in direction ν. Spatial difference operators d_ν^+ and d_ν^-, approximating ∂_ν, and an averaging operator μ_ν^- in direction ν may be defined as

$$d_\nu^+ = \frac{1}{X}\left(e_\nu^+ - 1\right) \quad d_\nu^- = \frac{1}{X}\left(1 - e_\nu^-\right) \quad \mu_\nu^- = \frac{1}{2}\left(1 + e_\nu^-\right) . \tag{44}$$

A centered approximation d_ν^η to a ηth derivative in coordinate ν may then be written as

$$d_\nu^\eta \triangleq \left(\mu_\nu^-\right)^{\alpha_\eta} \left(d_\nu^+\right)^{M_\eta + \alpha_\eta} \left(d_\nu^-\right)^{M_\eta} \approxeq \partial_\nu^\eta , \tag{45}$$

where η may be decomposed uniquely as $\eta = 2M_\eta + \alpha_\eta$ for integer M_η and α_η. This yields, from (13), a centered approximation $d_{l,m}$ to $D_{l,m}$:

$$d_{l,m} = \sum_{\boldsymbol{\eta}\in\mathbb{B}^l} \sigma_{l,m}^{(\boldsymbol{\eta})} \prod_{\nu=x,y,z} d_\nu^{\eta_\nu} \approxeq D_{l,m} . \tag{46}$$

Such approximations, when applied to the discrete Dirac approximation in (42), automatically satisfy necessary moment conditions[56]. Far more refined approximations to the Dirac delta function under differentiation are available[56,57], and allowing for optimised performance over a wide range of wavenumbers, and operation at locations not coincident with a grid location[32]. The choice above, however, is sparse, and, by virtue of centering, free of phase error. See Figure 2, illustrating the stencil of the discrete operator $d_{l,m}$ over a grid.

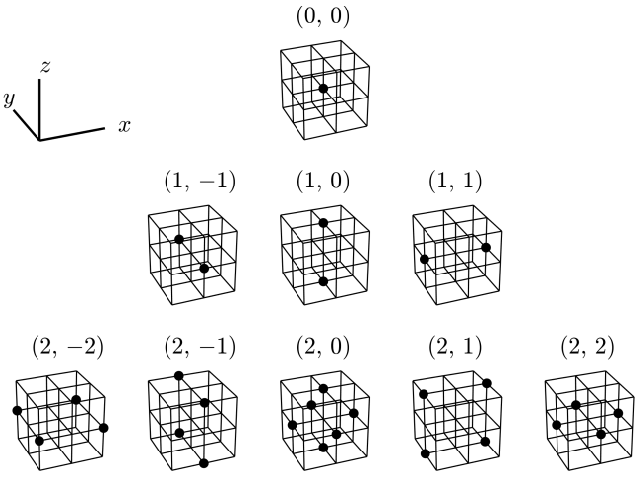

FIG. 2. Centered discrete stencils of the operator $d_{l,m}$, as defined in (46), for $l = 0, 1, 2$.

A discrete approximation to (14) is then

$$p_{\mathbf{q}}^{n+1} = 2p_{\mathbf{q}}^n - p_{\mathbf{q}}^{n-1} + \lambda^2 \sum_{\mathbf{e}\in\mathbb{Q}} \left(p_{\mathbf{q}+\mathbf{e}}^n - p_{\mathbf{q}}^n\right) \tag{47}$$

$$+T^2 \sum_{l=0}^{\infty} \sum_{m=-l}^{l} c^{l+2} f_{l,m}^n d_{l,m} s_{\mathbf{q}} ,$$

where $s_{\mathbf{q}}$ is the discrete Dirac delta function approximation from (42), under the action of the difference operators $d_{l,m}$, from (46). The discrete-time source signals $f^n_{l,m}$ are derived from an underlying scalar source signal f^n through convolution with the functions $a^n_{l,m}$:

$$f^n_{l,m} = a^n_{l,m} * f^n \,. \tag{48}$$

It is important to point out that the additional computational expense of the inclusion of a source term through scheme (47) above is minimal. The footprint of the discrete Dirac approximations is local and sparse, and the operation count is $O(L^4)$ additions/multiplications per sample for a maximal spherical harmonic order L. For a reasonable maximal order, the cost is many times smaller than that associated with running scheme (47) over the interior. This is in contrast to other proposed methods, which require large linear system solutions which may at present be computationally infeasible[31]. The other cost, when fitting to measured data, is in the offline fitting procedure—which is entirely independent of the FDTD scheme, and for which cost is generally not high. See Section IV.

C. Receivers

Receiver modeling is not the focus of this paper; yet, in Section V, directivity patterns from an FDTD scheme will be drawn from virtual omnidirectional receivers located on the surface of a sphere. Given that pressure values are only defined over the grid locations, some form of interpolation is necessary. Many varieties are available, but to ensure that additional error is minimized, a high-accuracy 10th-order optimised separable approximant, defined over a $10 \times 10 \times 10$ cube of grid points around the interpolation location is used[32].

VI. SIMULATION RESULTS

In this section, a variety of simulation results are presented, using the scheme (47) under different source configurations. All simulations are carried out at a sample rate of 44.1 kHz, over a cubic region of side length 2 m, centered at $\mathbf{r} = \mathbf{0}$, with the source located at the center at grid location $\mathbf{q} = \mathbf{0}$. The wave speed c is chosen as $c = 343$ m$\cdot$ s^{-1}. To simulate free-field conditions, absorbing boundary conditions (of second order Engquist-Majda type[58]) are employed at the faces of the cubic region.

For testing purposes, the source signals will take different forms depending on the application. For the generation of directivity patterns, a basic approximation to the temporal Dirac delta function will be used:

$$w^n_i = \begin{cases} 1, & n = 0 \\ 0, & n \geq 0 \end{cases} \,. \tag{49}$$

For plots of wave propagation, as in, e.g., Section VI B, a shifted unit amplitude Gaussian pulse of the form

$$w^n_g = \exp\left(-\frac{(nT - t_e)^2}{2\sigma^2} \right) \tag{50}$$

is used. Here, σ is the RMS width, and the shift t_e may be chosen as $t_e = \sigma\sqrt{-2\ln(\epsilon)}$ where ϵ represents machine epsilon ($\epsilon = 1.1 \times 10^{-16}$ in double precision floating point arithmetic). As the system is linear and time invariant, any necessary scaling to physical units and/or with respect to the time step for convergence testing may be carried out in post processing.

Note that the amplitudes of the functions $a_{l,m}$ (Eq. (15)) can decrease rapidly with increasing l. They are in the order of -100 dB $\cdot\, l$ for small sources that are centered at the expansion center. The numerical precision of the underlying computation system has to be commensurate. We are using double precision in all simulations presented below.

A. Individual Spherical Harmonic Directivity Patterns

As a first test, consider the response of the scheme (47) when only one spherical harmonic directivity pattern is activated. Thus, for a given choice of spherical harmonic (l_0, m_0), f^n and a_{l_0,m_0} are chosen as impulses w^n_i, from (49); all other responses $a_{l,m}$, $(l,m) \neq (l_0, m_0)$ are set to zero. The standard spherical harmonic directivity patterns are regenerated, here using an array of 1800 receivers (60 azimuthal by 30 in inclination) located on a sphere of radius 0.3 m. The receiver responses are Fourier transformed, and the magnitude response (normalised) at 2 kHz is illustrated in Figure 3, for spherical harmonics of order $l_0 \leq 2$.

Numerical dispersion effects, combined with truncation error in the discrete approximations to the operators $D_{l,m}$ lead to a deviation of the directivity from the ideal as frequency increases. See Figure 4. There are various remedies: operating at a higher sample rate is the simplest, but better designs both for the scheme itself[55], as well as for required approximations to the Dirac under spatial differentiation[32] are available.

B. The Displaced Monopole

Consider now the case of the displaced monopole, as described in Section III, for a source centered at coordinates $\mathbf{r}_0 = [0, -0.2, 0]$. Using the exact forms of the $a_{l,m}(t)$, from (32), sampled to yield time series $a^n_{l,m}$, and using a Gaussian source signal of the form $f^n = w^n_g$, with $\sigma = 2 \times 10^{-4}$, from (50). Snapshots of the time evolution of the pulse are shown in Fig. 5, using a maximal spherical harmonic order $L = 3$ at top, and for $L = 6$ at bottom. The plot clearly shows the presence of a virtual source away from the location of the driving term, indicated by a solid white circle. At grid locations near the driving location, over a region corresponding to the stencil of the source approximation for a given maximal order

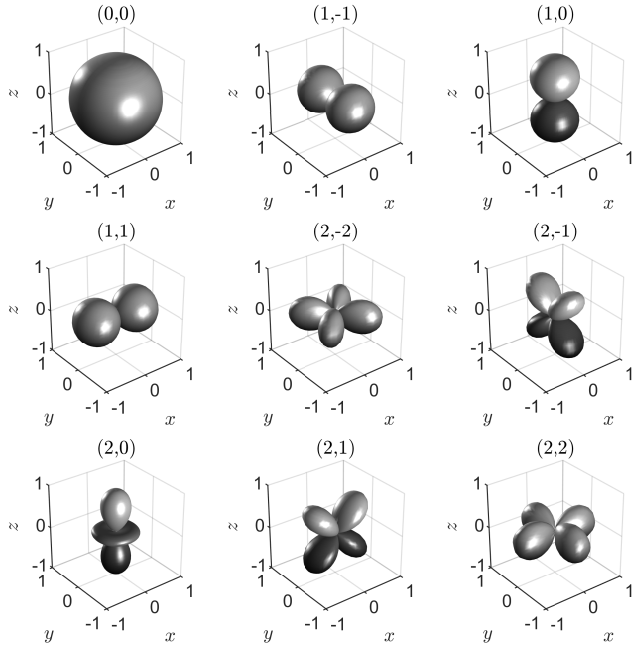

FIG. 3. Spherical harmonic directivity patterns (normalised), for $l \leq 2$ at 2 kHz generated by scheme (47).

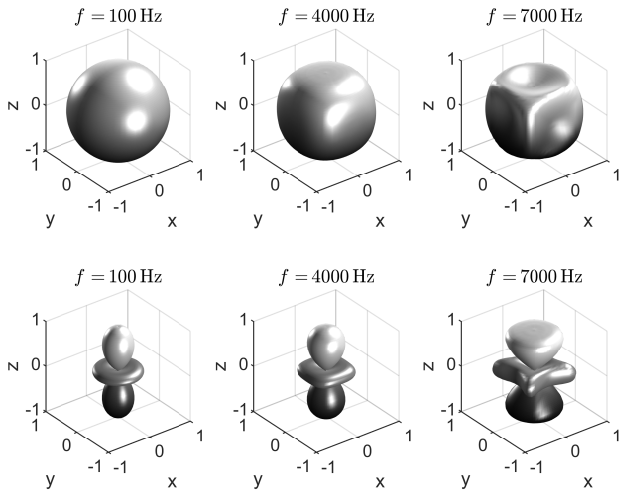

FIG. 4. Directivity patterns (normalised) for scheme (47) driven with a single spherical harmonic component, at frequencies as indicated, illustrating numerical inaccuracy with increasing frequency. Top row: $l = 0$, $m = 0$. Bottom row: $l = 2$, $m = 0$.

L, the computed field values will exhibit the pattern of the driving term itself; note however, that in the limit of high sample rates (meaning that T and X approach zero), the size of this region also decreases.

Fig. 6 shows the evolution of the acoustic field from Fig. 5 observed continuously over time at one location. The signals produced by FDTD match the exact order-limited signal obtained from the analytical expression (23). The exact signal (21) is shown for comparison.

C. Fitting to Measured Data: the IEM Loudspeaker Cube

Fig. 7 depicts the directivity patterns that were obtained based on the measured directivity of Loudspeaker 1 of the IEM loudspeaker cube[59,60]. The directivity was measured on 648 equi-angularly spaced points with a spacing of 10° on a spherical surface of radius 0.75 m. The propagation delay from the loudspeakers to the measurement surface is not contained in the impulse responses. A sufficient amount of silence was therefore pre-padded before the processing to maintain causality of the resulting functions $a_{l,m}$ as explained in Sec. IV. Loudspeaker data was chosen for this example in order to avoid the uncertainties that come with interpreting the data from musical instruments or the human voice or the like[10].

The spherical harmonic coefficients $\mathring{W}_{l,m}(R,\omega)$ were obtained through a non-regularized least squares fit to the complex spectral data for a maximal order of $L = 6$, as explained in Section IV. This order limitation makes the directivity as represented by the coefficients $\mathring{W}_{l,m}(R,\omega)$ deviate slightly from the measurement data. This is evident when comparing the top row in Fig. 7 to the middle row. The directivity that arises in the FDTD simulation matches the fitted directivity very well whereby small deviations occur at higher frequencies (middle row vs. bottom row).

VII. CONCLUDING REMARKS

The model presented here is intended as a flexible and general starting point for frequency-dependent directional source modeling in any volumetric wave-based time domain method. As such, it is presented directly in the continuous spatio-temporal domain. The representation in terms of differential operators associated with the spherical harmonic functions allows for a convenient means of fitting the model against measured directivity patterns, and a fitting procedure is demonstrated. Discretisation has been carried out here using conventional finite difference time domain methods over regular Cartesian grids. If one were to employ a different method, perhaps defined over an irregular grid arrangement (such as, e.g., a finite element method), the main change would be in the way in which the Dirac delta function and its derivatives are approximated over such a grid—the temporal filtering operations remain unchanged.

A great benefit of such a local source model is computational efficiency—as discussed in Section V B, the additional computational cost of such a source model is very small relative to the operation of the scheme over the problem interior. Another result of the locality of the source model is that it can be applied equally at any point in the problem domain without any recalculation of temporal filters or the Dirac approximations. These are advantages of volumetric wave-based approaches over meth-

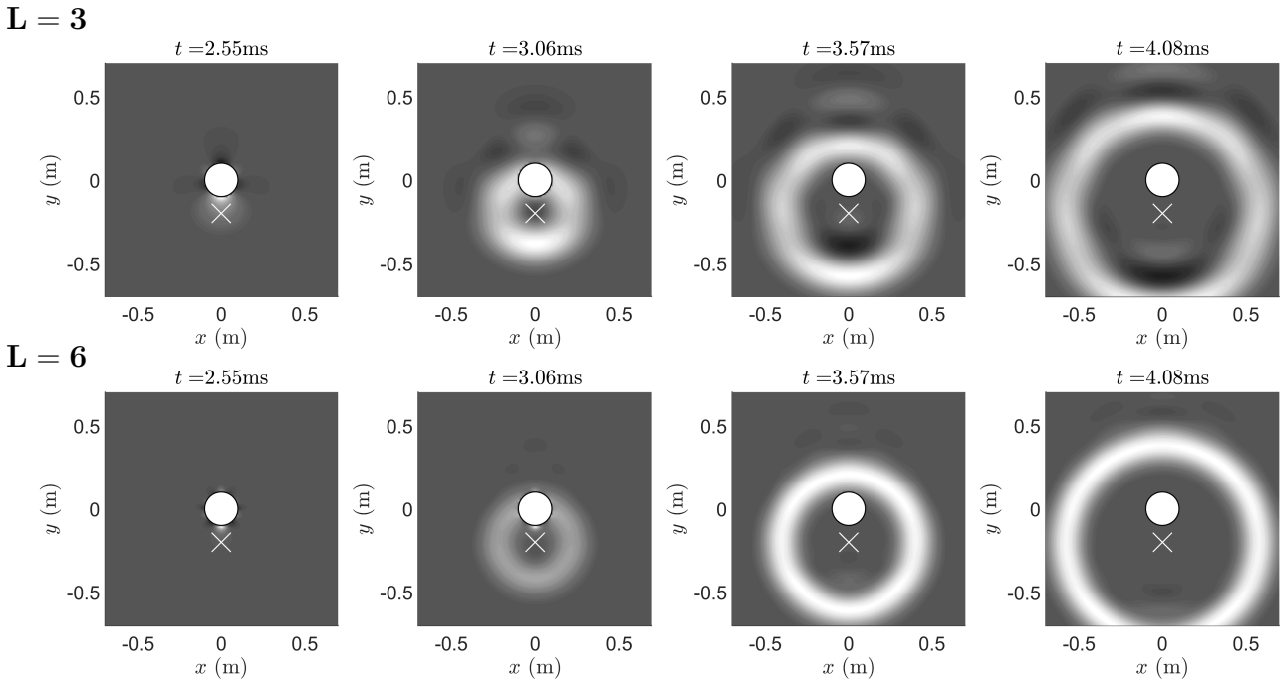

FIG. 5. Time evolution of the acoustic field, at times as indicated, for a displaced monopole source (centered at the cross), using a driving term located at the coordinate center (white circle). Results are shown using filters $a_{l,m}$ in (32) for a maximal spherical harmonic order $L = 3$ (top row) and $L = 6$ (bottom row).

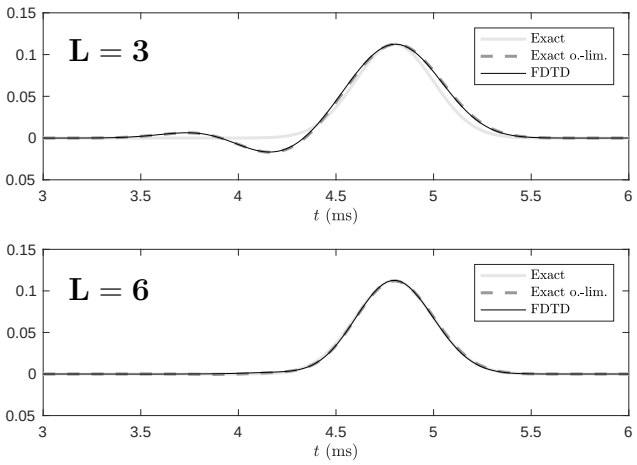

FIG. 6. The acoustic field from Fig. 5 observed at $\mathbf{r} = (0.5, 0.5, 0)$ m (solid black line) as well as the exact order-limited signal (dashed gray, (23) for $l \leq L$) and the exact signal (solid gray, (21)).

ods that operate over the room boundary, such as, e.g., equivalent source and boundary element methods, where the incorporation of source directivity requires a numerical integration over the room boundary[38,61], which will be dependent on the source location within the room. Indeed, as the model is locally defined and expressed entirely in the time domain, there is no impediment to the extension to the linear and time-varying case—i.e., of moving or rotating sources[32], which is a key feature in virtual acoustics applications. It is even possible to go further and emulate sources for which the directivity itself is time varying. There will be some additional cost required in recalculating interpolated approximations to $D_{l,m}$ in the run-time loop, but again, such a cost is very small relative to that of computation of the acoustic field over the problem interior. One possibility not discussed here is that of running multiple simulations, each with a single SH source directivity, which may then be recombined, in a post-processing stage, to yield source emulation of any desired directivity within an enclosure.

A real difficulty, and a subject worthy of future work, is the lack of a theoretical characterisation of the error of this spherical harmonic source model. Though, through consistency of the numerical approximation (47) with the model system (14), it is assured that the model is convergent (thus exhibiting the correct behaviour in the low frequency limit), a full analysis is complicated by the interaction of the dispersion error for the FDTD scheme itself over the interior, and the distinct approximation to the operators $D_{l,m}$. In practice, it appears that the model is indeed quite well-behaved over the low frequency range over which the FDTD scheme itself does not exhibit much dispersion, as clearly seen in Figure 4. The full characterisation of numerical directivity is complicated, however, by its spurious frequency and range dependence.

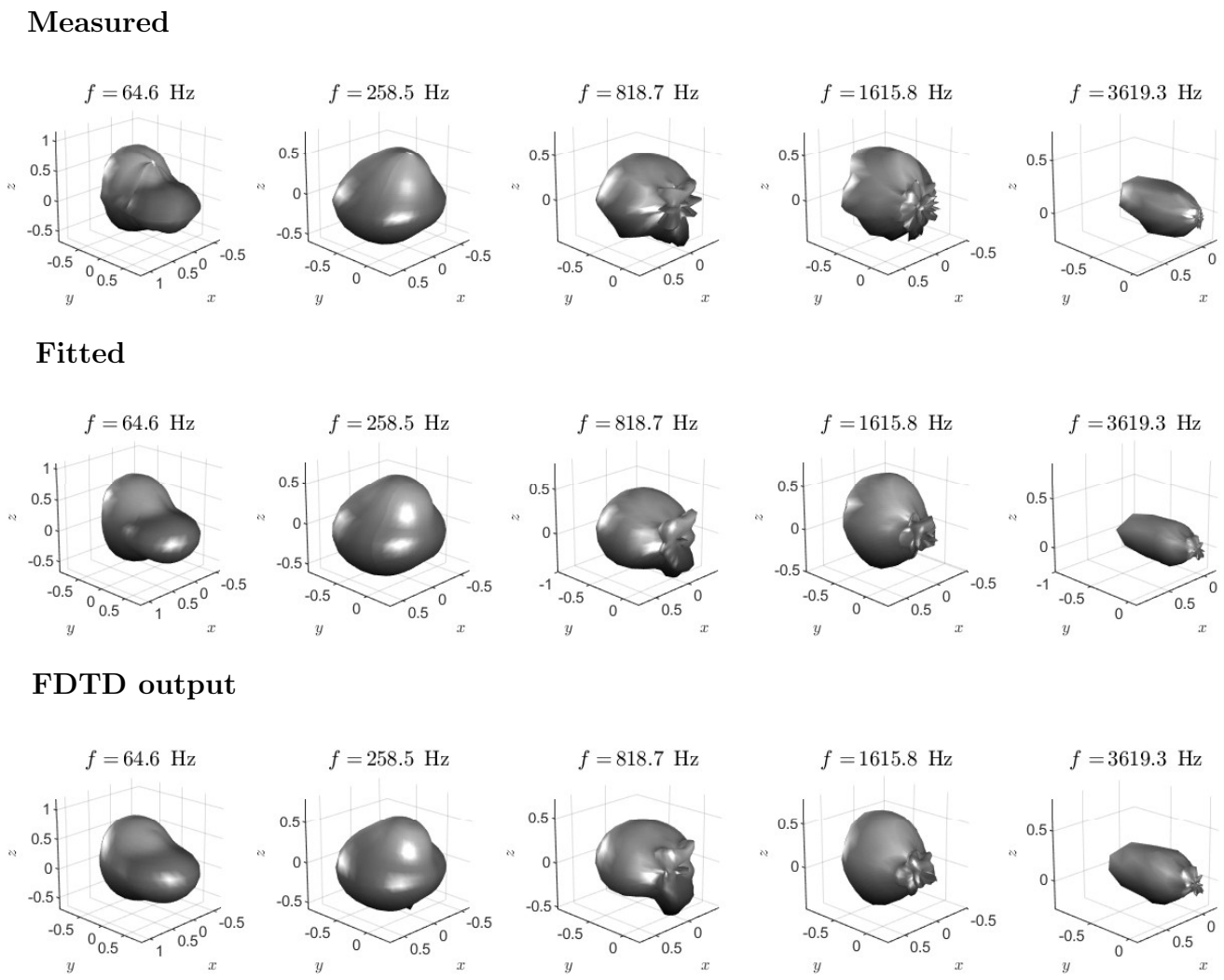

FIG. 7. Normalised directivity patterns, for Loudspeaker 1 of the IEM loudspeaker cube, at frequencies as indicated. Top row: measurement data. Middle row: reconstruction of directivity using filters $a_{l,m}$, up to maximal order $L = 6$. Bottom row: directivity from time domain output of scheme (47).

A pitfall of the spherical harmonic representation of the source is that it is only valid outside of a spherical volume that is centered at the coordinate origin and includes the source in its entire physical extent[47]. However, the physical extent of the sound source cannot be directly deduced from the spherical harmonics coefficients. It will therefore not be directly predictable how large the area around the expansion center will be in which the simulation will not be meaningful. One has to make sure that any boundary be outside of above defined spherical volume. But this concern is general, and not specific to the case of volumetric time domain methods.

The amount of currently available data on sound source directivities is very limited. The main reasons are that the measurement is resource intensive and the obtained data are somewhat limiting. It is simply not possible with most sound sources to play arbitrary and reproducible measurement signals through them. Also, the directivity can vary strongly with how the source is driven[5,10]. Future work will require deriving parametric methods to approximate and extrapolate measurement data such that they can be employed conveniently in virtual acoustics frameworks.

APPENDIX A: FOURIER TRANSFORMS

A temporal Fourier transform pair, for a function $g(t)$, $t \in \mathbb{R}$ and its transform $\hat{g}(\omega)$, $\omega \in \mathbb{R}$ is defined as

$$\hat{g}(\omega) = \int_{-\infty}^{\infty} g(t)\, e^{i\omega t} dt \qquad g(t) = \frac{1}{2\pi} \int_{-\infty}^{\infty} \hat{g}(\omega)\, e^{-i\omega t} d\omega\,. \tag{A1}$$

Note the sign convention, which follows that of, e.g., Williams[47]. This definition holds for functions of several variables, such as $p(\mathbf{r}, t)$, which transforms to $\hat{p}(\mathbf{r}, \omega)$.

A spatial Fourier transform pair, for a scalar function $g(\mathbf{r})$, $\mathbf{r} \in \mathbb{R}^3$ and its transform $\tilde{g}(\mathbf{k})$, $\mathbf{k} \in \mathbb{R}^3$ is defined as

$$\tilde{g}(\mathbf{k}) = \iiint_{\mathbb{R}^3} g(\mathbf{r}) e^{-i\mathbf{k}\cdot\mathbf{r}} d\mathbf{r} \tag{A2a}$$

$$g(\mathbf{r}) = \frac{1}{8\pi^3} \iiint_{\mathbb{R}^3} \tilde{g}(\mathbf{k}) e^{i\mathbf{k}\cdot\mathbf{r}} d\mathbf{k}\,, \tag{A2b}$$

where $d\mathbf{r}$ and $d\mathbf{k}$ are volume differential elements.

For a function g with spherical symmetry, so that $g = g(r)$, then $\tilde{g} = \tilde{g}(k)$, where $r = |\mathbf{r}|$ and $k = |\mathbf{k}|$, the transform pair is defined by

$$\tilde{g}(k) = 4\pi \int_0^\infty g(r) j_0(kr)\, r^2 dr \tag{A3a}$$

$$g(r) = \frac{1}{2\pi^2} \int_0^\infty \tilde{g}(k) j_0(kr)\, k^2 dk\,. \tag{A3b}$$

APPENDIX B: AN IDENTITY

In this appendix, the following identity is demonstrated:

$$D_{l,m} h_0^{(1)}(\omega r/c) = \left(-\frac{\omega}{c}\right)^l Y_{l,m}(\boldsymbol{\gamma})\, h_l^{(1)}(\omega r/c)\,, \tag{B1}$$

where $D_{l,m}$ is the spherical harmonic differential operator, as defined in (11), and where $h_l^{(1)}$ is the lth order spherical Hankel function of the first kind.

Consider the operator $D_{l,m}$ applied to a spherically-symmetric function $g(r)$, yielding $w_{l,m} = D_{l,m} g$. Under spatial Fourier transformation, from (A2a), one arrives at an expression for the spatial Fourier transform of $w_{l,m}(\mathbf{r})$:

$$\tilde{w}_{l,m}(\mathbf{k}) = \iiint_{\mathbb{R}^3} \left(D_{l,m} g(r)\right) e^{-i\mathbf{k}\cdot\mathbf{r}} d\mathbf{r}\,. \tag{B2}$$

Employing integration by parts l times for each term in $D_{l,m}$ leads to

$$\tilde{w}_{l,m}(\mathbf{k}) = (-1)^l \iiint_{\mathbb{R}^3} g(r) \left(D_{l,m} e^{-i\mathbf{k}\cdot\mathbf{r}}\right) d\mathbf{r}\,. \tag{B3}$$

But, because $D_{l,m}$ is homogeneous and of degree l, and using $\mathbf{k} = k\boldsymbol{\gamma}_\mathbf{k}$, where k is wavenumber, and $\boldsymbol{\gamma}_\mathbf{k}$ is a unit-length direction vector,

$$D_{l,m} e^{-i\mathbf{k}\cdot\mathbf{r}} = (-i)^l k^l Y_{l,m}(\boldsymbol{\gamma}_\mathbf{k})\, e^{-i\mathbf{k}\cdot\mathbf{r}} \tag{B4}$$

and thus

$$\tilde{w}_{l,m}(\mathbf{k}) = i^l k^l Y_{l,m}(\boldsymbol{\gamma}_\mathbf{k})\, \tilde{g}(k)\,. \tag{B5}$$

Inverse transforming, through (A2b) leads to

$$w_{l,m}(\mathbf{r}) = \frac{i^l}{8\pi^3} \int_0^\infty k^{2+l} \tilde{g}(k) \iint_{S^2} Y_{l,m}(\boldsymbol{\gamma}_\mathbf{k})\, e^{i\mathbf{k}\cdot\mathbf{r}} d\Omega dk\,. \tag{B6}$$

One may then employ the plane wave expansion[42]

$$e^{i\mathbf{k}\cdot\mathbf{r}} = 4\pi \sum_{l'=0}^{\infty} \sum_{m'=-l'}^{l'} i^{l'} j_{l'}(kr)\, Y_{l',m'}(\boldsymbol{\gamma}_\mathbf{k})\, Y_{l',m'}(\boldsymbol{\gamma}) \tag{B7}$$

in (B6), where $j_{l'}$ is the spherical Bessel function of order l'. Using the orthogonality of the spherical harmonics, from (9), one arrives at

$$w_{l,m}(\mathbf{r}) = Y_{l,m}(\boldsymbol{\gamma}) \frac{(-1)^l}{2\pi^2} \int_0^\infty k^{l+2} \tilde{g}(k)\, j_l(kr)\, dk\,. \tag{B8}$$

Consider now the identity

$$\{j_l(\zeta),\, h_l(\zeta)\} = (-1)^l \zeta^l \left(\frac{1}{\zeta}\frac{d}{d\zeta}\right)^l \{j_0(\zeta),\, h_0(\zeta)\}\,. \tag{B9}$$

This implies that

$$j_l(kr) = (-1)^l \frac{r^l}{k^l} \left(\frac{1}{r}\frac{\partial}{\partial r}\right)^l j_0(kr)\,. \tag{B10}$$

Inserting this identity into (B8), and employing $j_0(kr) = \sin(kr)/kr$, as well as the inverse spatial Fourier transformation for spherically symmetric functions, from (A3b) leads, finally, to

$$w_{l,m}(\mathbf{r}) = D_{l,m} g(r) = Y_{l,m}(\boldsymbol{\gamma})\, r^l \left(\frac{1}{r}\frac{d}{dr}\right)^l g(r)\,. \tag{B11}$$

Now, using $g(r) = h_0^{(1)}(\omega r/c)$, as well as identity (B9) leads to (B1).

[1] D. Poirer-Quinot, B. Katz, and M. Noisternig, "EVERTims: Open source framework for real-time auralization in architectural acoustics and virtual reality," in *Proceedings of the 20th International Conference on Digital Audio Effects*, Edinburgh, UK (2017), pp. 323–328.

[2] CLF Group, "Common loudspeaker format," Available online at http://www.clfgroup.org/ (Last viewed 06/05/2019) (2019).

[3] L. Savioja and U. P. Svensson, "Overview of geometrical room acoustic modeling techniques," J. Acoust. Soc. Am. **138**(2), 708–730 (2015).

[4] G. Weinreich and E. B. Arnold, "Method for measuring acoustic radiation fields," J. Acoust. Soc. Am. **68**(2), 404–411 (1980).

[5] F. Zotter, "Analysis and synthesis of sound-radiation with spherical arrays," Ph.D. thesis, University of Music and Performing Arts, Austria, 2009.

[6] D. Malham, "Spherical Harmonic Coding of Sound Objects - the Ambisonic 'O' Format," in *19th International Conference of the AES, paper 1919*, Schloss Elmau, Germany (2001).

[7] D. Menzies, "W-Panning and O-Format, Tools for Object Spatialization," in *22nd International Conference of the AES, paper 000225*, Espoo, Finland (2002).

[8] A. Wabnitz, N. Epain, C. Jin, and A. van Schaik, "Room acoustics simulation for multichannel microphone arrays," in *Proceedings of the International Symposium on Room Acoustics*, Melbourne, Australia (2010).

[9] D. Schröder, "Physically based real-time auralization of interactive virtual environments," Ph.D. thesis, Aachen University, 2011.

[10] N. R. Shabtai, G. Behler, M. Vorländer, and S. Weinzierl, "Generation and analysis of an acoustic radiation pattern database for forty-one musical instruments," J. Acoust. Soc. Am. **141**(2), 1246–1256 (2017).

[11]M. Pollow, *Directivity Patterns for Room Acoustical Measurements and Simulations* (Logos Verlag Berlin GmbH, Berlin, 2015).

[12]P. N. Samarasinghe, T. D. Abhayapala, Y. Lu, H. Chen, and G. Dickins, "Spherical harmonics based generalized image source method for simulating room acoustics," J. Acoust. Soc. Am. **144**(3), 1381–1391 (2018).

[13]O. Chiba, T. Kashiwa, H. Shimoda, S. Kagami, and I. Fukai, "Analysis of sound fields in three dimensional space by the time-dependent finite-difference method based on the leap frog algorithm," J. Acoust. Soc. Jpn.(J) **49**, 551–562 (1993).

[14]L. Savioja, T. Rinne, and T. Takala, "Simulation of room acoustics with a 3-D finite-difference mesh," in *Proc. Int. Comp. Music Conf.*, Århus, Denmark (1994), pp. 463–466.

[15]D. Botteldooren, "Acoustical finite-difference time-domain simulation in a quasi-cartesian grid," J. Acoust. Soc. Am. **95**(5), 2313–2319 (1994).

[16]D. Botteldooren, "Finite-difference time-domain simulation of low-frequency room acoustic problems," J. Acoust. Soc. Am. **98**(6), 3302–3308 (1995).

[17]S. Bilbao, "Modeling of complex geometries and boundary conditions in finite difference/finite volume time domain room acoustics simulation," IEEE Trans. Audio Speech Language Proces. **21**(7), 1524–1533 (2013).

[18]S. Bilbao, B. Hamilton, J. Botts, and L. Savioja, "Finite volume time domain room acoustics simulation under general impedance boundary conditions," IEEE/ACM Trans. Audio Speech Language Proces. **24**(1), 161–173 (2016).

[19]M. Hornikx, W. De Roeck, and W. Desmet, "A multi-domain Fourier pseudospectral time-domain method for the linearized Euler equations," J. Comp. Phys. **231**(14), 4759–4774 (2012).

[20]R. Mehra, N. Raghuvanshi, L. Savioja, M. Lin, and D. Manocha, "An efficient GPU-based time domain solver for the acoustic wave equation," Appl. Acoust. **73**(2), 83–94 (2012).

[21]D. Murphy, A. Kelloniemi, J. Mullen, and S. Shelley, "Acoustic modelling using the digital waveguide mesh," IEEE Sig. Proc. Mag. **24**(2), 55–66 (2007).

[22]Y. Yasuda and T. Sakuma, "Boundary element method," in *Computational Simulation in Architectural and Environmental Acoustics*, edited by T. Sakuma, S. Sakamoto, and T. Otsuru (Springer, 2014), p. 80.

[23]A. Celestinos and S. Nielsen, "Low-frequency loudspeaker room simulation using finite differences in the time domain part 1: Analysis," J. Audio Eng. Soc. **56**(10), 772–786 (2008).

[24]J. Botts, A. Bockman, and N. Xiang, "On the selection and implementation of sources for finite-difference methods," in *Proc. 20th Int. Congr. Acoust.*, Sydney, Australia (2010).

[25]H. Jeong and Y. Lam, "Source implementation to eliminate low-frequency artifacts in finite difference time domain room acoustic simulation," J. Acoust. Soc. Am. **258–268**(1), 1112–1118 (2012).

[26]A. Southern and D. Murphy, "Low complexity directional sound sources for finite difference time domain room acoustic models," in *Proc. 126th Audio Eng. Soc. Conv.*, Munich, Germany (2009).

[27]J. Sheaffer, M. van Walstijn, and B. Fazenda, "Physical and numerical constraints in source modeling for finite difference simulation of room acoustics," J. Acoust. Soc. Am. **135**(1) (2014).

[28]D. Murphy, A. Southern, and L. Savioja, "Source excitation strategies for obtaining impulse responses in finite difference time domain room acoustics simulation," Appl. Acoust. **82**, 6–14 (2014).

[29]J. Schneider, C. Wagner, and S. Broschat, "Implementation of transparent sources embedded in acoustic finite-difference time domain grids," J. Acoust. Soc. Am. **136–142**(1), 3219–3226 (1998).

[30]J. Escolano, J. Lopez, and B. Pueo, "Directive sources in acoustic discrete-time domain simulations based on directivity diagrams," JASA Express Lett. **121**, 256–262 (2007).

[31]D. Takeuchi, K. Yatabe, and Y. Oikawa, "Source directivity approximation for finite-difference time-domain simulation by estimating initial value," J. Acoust. Soc. Am. **145**(4), 2638–2649 (2019).

[32]S. Bilbao and B. Hamilton, "Directional sources in wave-based acoustic simulation," IEEE Trans. Audio Speech Language Proces. **27**, 415–428 (2019).

[33]M. Bencomo and W. Symes, "Discretization of multipole sources in a finite difference setting for wave propagation problems," J. Comp. Phys. **386**, 296 – 322 (2019).

[34]G. Dickins and R. Kennedy, "Towards optimal soundfield representation," in *Proc. Audio Eng. Soc. Conv.*, Munich, Germany (1999), paper 4925.

[35]G. Dickins, "Soundfield representation, reconstruction and perception," M.Sc. thesis, Australian National University (2003).

[36]E. Rowe, "Spherical delta functions and multipole expansions," J. Math. Phys. **19**, 1962–1968 (1978).

[37]S. Bilbao, A. Politis, and B. Hamilton, "Local time-domain spherical harmonic spatial encoding for wave-based acoustic simulation," IEEE Signal Proces. Lett. **26**(4), 617–621 (2019).

[38]R. Mehra, L. Antani, S. Kim, and D. Manocha, "Source and listener directivity for interactive wave-based sound propagation," IEEE Trans. Visualization Comp. Graphics **20**(4), 83–94 (2014).

[39]N. Gumerov and R. Duraiswami, *Fast Multipole Methods for the Helmholtz Equation in Three Dimensions* (Elsevier, Amsterdam, The Netherlands, 2004).

[40]A. Pierce, *Acoustics: An introduction to its physical principles and applications* (Acoustical Society of America, 1991).

[41]J. Ahrens, *Analytic Methods of Sound Field Synthesis* (Springer, Heidelberg, Germany, 2012), p. 30.

[42]B. Rafaely, *Fundamentals of Spherical Array Processing* (Springer, New York, 2015).

[43]P. Cotterell, "On the theory of the second order soundfield microphone," Ph.D. thesis, University of Reading, 2002.

[44]N. Hahn and S. Spors, "Time domain representations of a plane wave with spatial band-limitation in the spherical harmonics domain," in *Proceedings of the Meeting of the German Acoustical Society (DAGA)*, Rostock, Germany (2019).

[45]J. Meyer, *Acoustics and the Performance of Music* (Springer, New York, 2009), p. 130.

[46]D. T. Blackstock, *Fundamentals of Physical Acoustics* (Wiley-Interscience, New York, NY, 2000), p. 495.

[47]E. Williams, *Fourier Acoustics: Sound Radiation and Nearfield Acoustical Holography* (Academic Press, New York, 1999).

[48]J. Daniel, "Spatial Sound Encoding Including Near Field Effect: Introducing Distance Coding Filters and a Viable, New Ambisonic Format," in *23rd International Conference of the AES, paper 16*, Espoo, Finland (2003).

[49]H. Pomberger, "Angular and radial directivity control for spherical loudspeaker arrays," Diploma thesis, University of Music and Dramatic Arts, Graz (2008).

[50]K. Atkinson and W. Han, *Spherical Harmonics and Approximations on the Unit Sphere: An Introduction* (Springer, Heidelberg, 2012), p. 204.

[51]J. Ahrens, M. R. P. Thomas, and I. Tashev, "HRTF magnitude modeling using a non-regularized least-squares fit of spherical harmonics coefficients on incomplete data," in *Proceedings of The 2012 Asia Pacific Signal and Information Processing Association Annual Summit and Conference (APSIPA)*, Hollywood, CA, USA (2012), pp. 1–5.

[52]S. Boyd and L. Vandenberghe, *Convex Optimization* (Cambridge University Press, Cambridge, UK, 2004), p. 649.

[53]R. Courant, K. Friedrichs, and H. Lewy, "On the partial differential equations of mathematical physics," Mathematische Annalen **100**, 32–74 (1928).

[54]J. Strikwerda, *Finite Difference Schemes and Partial Differential Equations* (Wadsworth and Brooks/Cole Advanced Books and Software, Pacific Grove, California, 1989).

[55]S. Bilbao and B. Hamilton, "Higher-order accurate two-step finite difference schemes for the many dimensional wave equation," J. Comp. Phys. **367**, 134–165 (2018).

[56]Y. Liu and Y. Mori, "Properties of discrete delta functions and local convergence of the immersed boundary method," SIAM J. Numer. Anal. **50**(6), 2986–3015 (2012).

[57]B. Hosseini, N. Nigam, and J. Stockie, "On regularizations of the Dirac delta distribution," J. Comp. Phys. **305**, 423–447 (2016).

[58]B. Engquist and A. Majda, "Absorbing boundary conditions for the numerical evaluation of waves," Math. Comp. **31**(139), 629–651 (1997).

[59]N. Meyer-Kahlen, F. Zotter, and K. Pollack, "Design and measurement of first-order, horizontally beam-controlling loudspeaker cube," in *144th Convention of the AES, e-Brief 447*, Milan, Italy (2018).

[60]F. Zotter, "High-resolution directional impulse responses of the iem loudspeaker cubes," Available online at https://phaidra.kug.ac.at/detail_object/o:70240 (Last viewed 06/05/2019) (2019).

[61]J. Hargreaves, L. Rendell, and Y. Lam, "A framework for auralization of boundary element method simulations including source and receiver directivity," J. Acoust. Soc. Am. **145**(4), 2625–2637 (2019).